12th International Symposium on Turbulence and Shear Flow Phenomena (TSFP12)
Osaka, Japan, July 19–22, 2022

BOUNDARY LAYER TRANSITION IN SONIC CONVERGING-DIVERGING NOZZLES

Bruno Zebrowski
Department of Fluid, Thermal and Combustion
Institut Pprime - CNRS, ENSMA
86962 Chasseneuil-du-Poitou, France
bruno.zebrowski@ensma.fr

Peter Jordan
Department of Fluid, Thermal and Combustion
Institut Pprime - CNRS, Université de Poitiers
86962 Chasseneuil-du-Poitou, France
peter.jordan@univ-poitiers.fr

Vincent Jaunet
Department of Fluid, Thermal and Combustion
Institut Pprime - CNRS, ENSMA
86962 Chasseneuil-du-Poitou, France
vincent.jaunet@ensma.fr

ABSTRACT

We study the laminar-to-turbulent boundary layer transition of converging-diverging sonic nozzles used as standard flow meters. Stability characteristics are addressed using the linear stability framework under the parallel flow assumption. We show that the boundary layer is stable to modal disturbances but can experience transient-growth of energy in the form of streaks of high and low velocity. The peak of energy associated to transient-growth is expected to happen within the throat region of the nozzle.

Transition trends are investigated using N factors. A higher acceleration associated with a small inlet radius tends to stabilise the non-modal mechanism. Freestream turbulence and surface roughness are discussed as possible receptivity mechanisms for transient-growth to occur. It is shown that roughness is unlikely to trigger the transition process.

INTRODUCTION

This work is motivated by boundary layer transition that occurs in converging-diverging sonic nozzles used in industrial applications as flow meters. The boundary layer displacement thickness at the nozzle throat influences the mass flow rate by reducing the effective sonic area. In standard discharge-coefficient models used to calibrate flow meters, laminar and turbulent boundary layer models were established for a set of nozzle shapes by Stratford (1964) and Geropp (1971). However, there is little information about the transitional regime, introducing uncertainty about the validity range of these models.

A common approach to study boundary layer transition is based on modal growth of infinitesimal disturbances on a linearised base flow. The boundary layer in the converging section of the nozzle ranges from subsonic to transonic. For a flat plate in a transonic regime, modal transition is characterized by a Tollmiens-Schlichting (T.S.) wave that is most unstable for plane 2D wave (Mack (1984) and Özgen & Kircali (2008)). However, a favourable pressure gradient is known to have a stabilizing effect on this mode Masad & Zurigat (1994)). Boundary layers are also subject to transient growth (Hanifi *et al.* (1996), Tumin & Reshotko (2001)), where streamwise vortices result in the formation of streaks of high and low streamwise velocity via the lift-up.

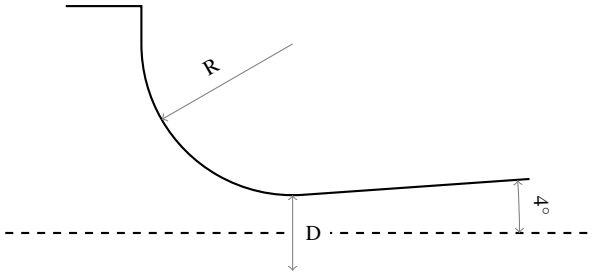

Figure 1. Sketch of the nozzle geometry under investigation

We investigate the stability characteristics of boundary layers in nozzles with an arc-circle throat shown in Figure 1, similar to those used as references in high-pressure mass flow rate applications. We first present the model used to obtain boundary layers for such flows that will be used as base flow. We investigate the spatial modal stability using the linear stability analysis framework for a compressible boundary layer. Then, we study non-modal mechanisms through transient growth analysis. N factors are computed and compared with literature data. The analysis is extended to other nozzle geometries by varying the ratio R/D. Finally, the roughness-induced transition is discussed based on the numerical simulation database of Bernardini *et al.* (2014) and through measurements of an analogous surface.

BASE FLOW

The boundary layer is modelled using the analytic solution proposed by Geropp (1971). The model is based on the compressible boundary layer equations with pressure gradient and an adiabatic wall. The equations are simplified by introducing the Prandtl number of unity and by using a linear relation between viscosity and temperature instead of the classical Sutherland's formula. The equations are worked out by in-

troducing self-similar velocity profiles that can be set for any given nozzle geometry by evaluating the streamwise pressure gradient at the nozzle throat. At the nozzle throat, the boundary layer equation is

$$y = \frac{D\left(\frac{\gamma+1}{2}\right)^{\frac{\gamma+1}{4(\gamma-1)}}}{\sqrt{R_0 m}\left(1-\frac{\gamma-1}{\gamma+1}\right)^{\frac{1}{2(\gamma-1)}}}\left[\sqrt{2}\,\mathrm{atanh}\sqrt{\frac{2+u/u_\delta}{3}} - \sqrt{2}\,\mathrm{atanh}\sqrt{\frac{2}{3}} + \frac{\frac{\gamma-1}{\gamma+1}}{1-\frac{\gamma-1}{\gamma+1}}\left[\frac{2}{\sqrt{3}} - \sqrt{\frac{2}{3}}\left(1-\frac{u}{u_\delta}\right)\sqrt{\frac{u}{u_\delta}+2}\right]\right], \quad (1)$$

where y is the wall normal position for a given value of velocity u/u_δ, where the value of $u/u_\delta \in [0,1]$, $R_0 = a_0 D/\nu_0$ is a stagnation-based Reynolds number with a_0 the stagnation speed of sound, D the nozzle throat diameter, ν_0 the kinematic viscosity at rest, M the Mach number, γ is the isentropic exponent and the subscript $_\delta$ denotes the value at the boundary layer edge. The acceleration parameter m is here chosen so that it has the same pressure gradient at the throat as a nozzle with an arc-circle throat

$$m = \frac{\sqrt{\frac{4}{\gamma+1}\frac{D}{R}}}{\left(\frac{\gamma+1}{2}\right)^{\frac{1-2\gamma}{\gamma-1}}}, \quad (2)$$

where R is the radius of the nozzle profile at the throat. In Equation 1, the boundary layer scales with the Reynolds number R_0 and the acceleration parameter m. As a result, the velocity profile shown in Figure 2 is self-similar and holds for any ratio R/D. In order to facilitate comparison with available data in the literature, we will use a Reynolds number based on the nozzle throat diameter

$$Re_t = \frac{\rho_\delta u_\delta D}{\mu_0}, \quad (3)$$

where μ_0 is the stagnation viscosity.

In the following, unless otherwise specified, the nozzle is chosen with a ratio $R/D = 2$, corresponding to the most commonly used nozzle geometry for mass flow measurement discussed in the introduction. The throat Reynolds number is set at $Re_t = 10^6$, corresponding to conditions where the transition is commonly observed.

STABILITY ANALYSIS

To perform the stability investigation, the compressible Navier-Stokes (N.-S.) equations are linearised by introducing the decomposition $\mathbf{q} = \bar{\mathbf{q}} + \mathbf{q}'$, where the state vector $\mathbf{q} = [\rho, u, v, w, T]^\top$ contains the density, the 3 velocity components and the temperature, $\mathbf{q}'$ is the state vector of fluctuating quantities and $\bar{\mathbf{q}}$ the base state. Under the small perturbation assumption, the linearised N.-S. equations are obtained

$$\frac{\partial}{\partial t}\mathbf{q}' = \mathbf{L}\mathbf{q}'. \quad (4)$$

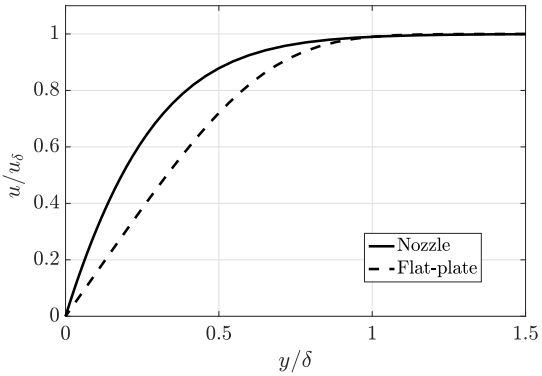

Figure 2. Boundary layer velocity profile in nozzle. Comparison between Geropp self-similar model and Blasius flat plate solution.

The linearised N.-S. operator $\mathbf{L}$ is further simplified by considering a locally parallel baseflow where the wall-normal direction is inhomogenous

$$\bar{\mathbf{q}}(x,y,z,t) = \bar{\mathbf{q}}(y), \quad (5)$$

The density and temperature are made non-dimensional by their reference values at the boundary layer edge δ and the velocities by the speed of sound outside the boundary layer c_δ. The reference length is the boundary layer displacement thickness δ^*. The corresponding Reynolds number is

$$Re_{\delta^*} = \frac{\bar{\rho}_\delta \bar{u}_\delta \delta^*}{\bar{\mu}_\delta} \quad (6)$$

For a nozzle with $R/D = 2$ at $Re_t = 10^6$, the computed displacement thickness-based Reynolds number is $Re_{\delta^*} = 1057$.

Spatial modal stability

The spatial modal stability of the boundary layer is adressed by considering the normal-mode ansatz

$$\mathbf{q}'(x,y,z,t) = \hat{\mathbf{q}}(y)\mathrm{e}^{i(\alpha x+\beta z-\omega t)}, \quad (7)$$

where α and β are the streamwise and spanwise wavenumbers and ω the frequency. In matrix form, the perturbation equation is

$$-i\omega\hat{\mathbf{q}} = \left[\mathbf{A_0}(\beta) + \mathbf{A_x}(\beta)\alpha + \mathbf{A_{xx}}\alpha^2\right]\hat{\mathbf{q}}. \quad (8)$$

with $\alpha \in \mathbb{C}$, $\beta \in \mathbb{R}$ and $\omega \in \mathbb{R}$. The matrices $\mathbf{A_0}$, $\mathbf{A_x}$ and $\mathbf{A_{xx}}$ are the constant coefficients of the linearised N.-S. equations. The polynomial eigenvalue problem in Equation 8 is solved for prescribed values of β and ω. Only the downstream-propagating modes are retained by applying the Briggs-Bers criterion (Briggs (1964) and Bers (1983)). The stability of the resulting eigenvalues α is given by Equation 7.

The eigenvalue problem is solved for pairs of wavenumbers varying from $\beta = [0,3]$ and $\omega = [0,3]$. Figure 3 presents a map of minimum imaginary part over all eigenvalues found

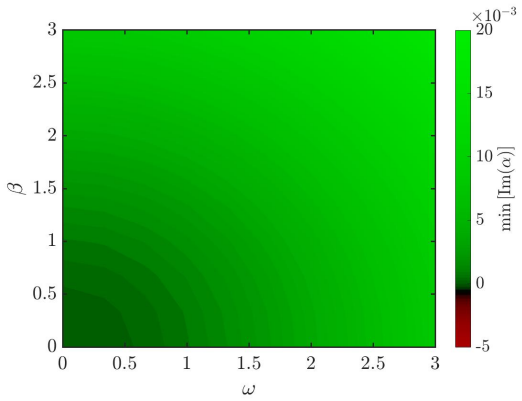

Figure 3. Map of Imaginary part of α at $Re^*_\delta = 1057$.

for each computed pair of $[\beta, \omega]$, where acoustic modes have been filterd out. For each pair of wavenumbers we have that $\min(\Im(\alpha)) > 0$. Since we have only kept the downstream-travelling modes, it shows that the flow is modally stable. In flows without pressure gradient, the Tollmien-Schlichting wave is unstable. In the present case, it is stabilised by the favorable pressure gradient, as illustrated in Figure 4.

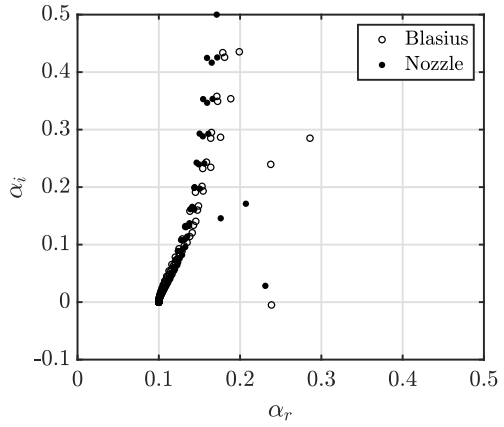

Figure 4. Spatial eigenspectrums for $\beta = 0$, $\omega = 0.1$ and $Re_{\delta^*} = 1057$. Comparison of Blasius B.L. without pressure gradient and the current nozzle B.L. with favorable pressure gradient.

This has been repeated for higher Reynolds numbers (up to $\mathrm{Re_t} = 10^7$) and the same conclusions have been drawn. We therefore conclude that the boundary layer in the choked region of the nozzle considered is modally stable, and transition must therefore be underpinned by non-modal mechanisms.

Spatial non-modal growth

Despite a stable modal behavior, transient-growth occurs due to the non-orthogonality of the linear operator $\mathbf{L}$. If small perturbations experience enough growth before decaying, they may either affect the base flow $\bar{\mathbf{q}}$ in a new modally unstable state or trigger nonlinear terms leading to turbulence.

The transient-growth analysis is performed by considering the normal-mode ansatz

$$\mathbf{q}'(x,y,z,t) = \hat{\mathbf{q}}(x,y)\mathrm{e}^{i(\beta z - \omega t)}, \tag{9}$$

and the resulting perturbation equation

$$-i\omega\hat{\mathbf{q}} = \mathscr{L}\hat{\mathbf{q}} = \left[\mathbf{A_0}(\beta) + \mathbf{A_1}(\beta)\frac{\partial}{\partial x} + \mathbf{A_2}\frac{\partial^2}{\partial x^2}\right]\hat{\mathbf{q}}. \tag{10}$$

The solution to Equation 10 is sought in the form

$$\hat{\mathbf{q}}(x,y) = \hat{\mathbf{q_0}}(y)\mathrm{e}^{\mathscr{L}x} \tag{11}$$

where $\hat{\mathbf{q_0}}(y) = \hat{\mathbf{q}}(y, x=0)$ is an initial small pertubation vector. The spatial growth of an initial perturbation is given by

$$\mathbf{G}(x,\beta,\omega) = \frac{\|\hat{\mathbf{q}}(x)\|^2_E}{\|\hat{\mathbf{q_0}}\|^2_E}. \tag{12}$$

where $\mathbf{G}$ is the gain, defined as the energy norm of the perturbation at a given x-location $\hat{\mathbf{q}}(x)$ produced by an initial disturbance $\hat{\mathbf{q}}_0$ over the energy norm of that same inital disturbance. Following the work of Chu (1965), the energy norm is chosen for the inner product $\langle \mathbf{q}, \mathbf{q} \rangle_E = \mathbf{q}^H \mathbf{W}_e \mathbf{q}$

$$\mathbf{W}_e = \mathrm{Diag}\left(\frac{\bar{T}}{\bar{\rho}\gamma}, \bar{\rho}, \bar{\rho}, \bar{\rho}, \frac{\bar{\rho}}{\bar{T}\gamma(\gamma-1)}\right). \tag{13}$$

Equation 12 is solved using optimal perturbations by performing the singular value decomposition of the matrix $\mathrm{e}^{\mathscr{L}x}$ after application of the energy norm. The detailed method to obtain the gain can be found in Jordan *et al.* (2017).

Spatial non-modal growth is computed for $\omega \in [0, 0.5]$ and $\beta \in [0, 2.5]$ for a total of 2500 pairs. The highest gain achieved over distance

$$\mathrm{G_{max}}(\omega,\beta) = \max_x \mathrm{G}(\omega,\beta,x). \tag{14}$$

is presented on Figure 5. It is shown that significant transient-

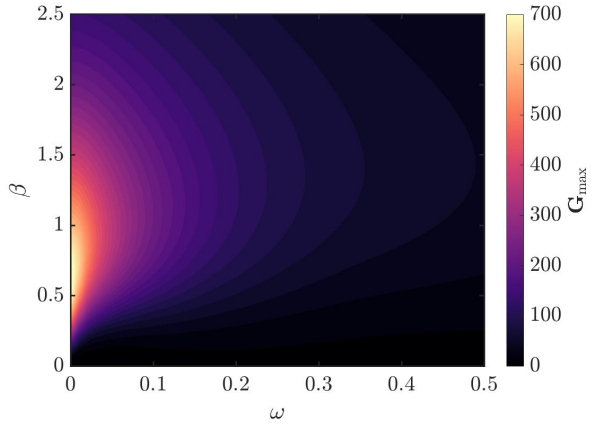

Figure 5. $\mathbf{G}_{\max}$ map at $Re^*_\delta = 1057$.

growth occurs for $\omega = 0$, corresponding to an optimal perturbation made of streamwise vortices leading to steady streaks of high and low velocity. The highest gain is acheived at $\beta \sim 0.61$ and $\omega = 0$. In general, high gains are confined at low frequencies ω and spanwise wavenumbers $\beta \in [0.4 - 1]$.

TRANSITION CHARACTERISTIC

The gain is found to scale with the Reynolds number as well as the spatial length of development, as mentionned in the calculation of Tumin & Reshotko (2001). In the case of the nozzle boundary layer, it is found that the dimensional length of development x^* scales with the throat diameter. The ratio R/D also modifies the boundary layer displacement thickness at the nozzle throat, therefore the length of streaks development is also affected by this ratio. Gains are presented in Figure 6 for various R/D. The highest gain are achieved at the optimal distance x^*_{opt} between $0.4D$ and $0.9D$, depending on R/D, for $\omega = 0$ and $\beta = 0.61$.

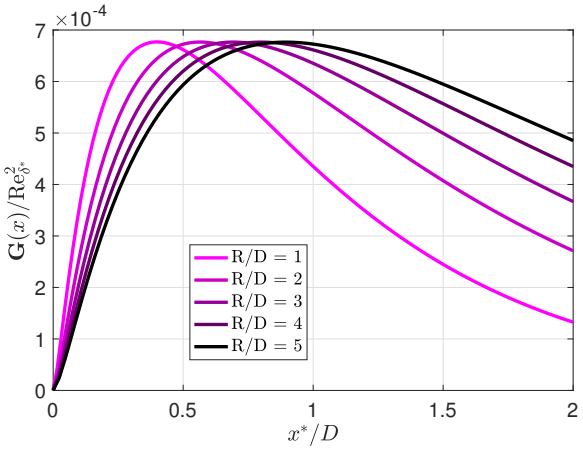

Figure 6. Spatial Gain $\mathrm{G}(\omega = 0, \beta = 0.61)$ scaled with Reynolds number. The distance is expressed in throat diameter, x^*/D and is independent of Reynolds number.

These optimal lengths indicates that the peak of energy will occur in the throat region. This makes the non-modal spatial growth a plausible candidate to explain the transition in these accelerated transonic flows.

N factors

The relations found between the gain, the Reynolds number and R/D allow to compute N factors

$$N = \ln(G_{max}) \tag{15}$$

to predict the trend of transition in a parametric study. The N factor is a parameter used to correlate the turbulence intensity of the freestream flow to the transition. It is commonly applied to the exponential growth of unstable mode on flat plate boundary layers. Since the present model is based on non-modal growth, the N factor cannot be directly compared with flat plate boundary layers. However, the N factors can be presented alongside experimental discharge coefficients obtained for the same nozzle geometry. We base the reference point on the experiments carried by Ishibashi (2015), in which the discharge coefficient is measured for a nozzle of $R/D = 2$. In Figure 7, it is compared the discharge coefficient obtained by Ishibashi from experimental data and the N factor computed by the present method for the same nozzle. As the Reynolds number increases, the discharge coefficient approaches unity as a result of a thinner boundary layer at the nozzle throat.

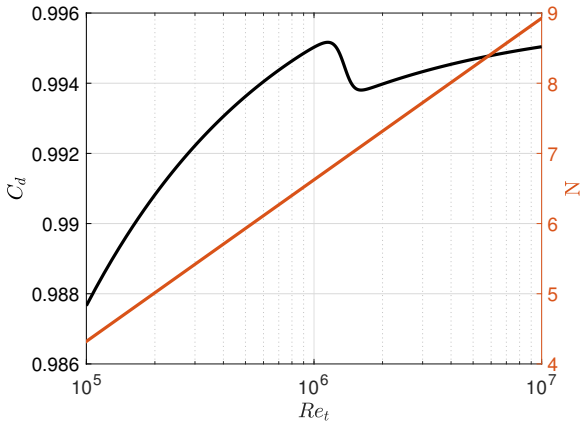

Figure 7. Discharge coefficient (Cd): black curve (left axis) and N factor: orange curve (right axis) as function of throat based Reynolds number Re_t. The discharge coefficient is a fit of experimental data for a nozzle of $R/D = 2$ (see Ishibashi (2015)).

From $Re_t = 10^5$ to $Re_t = 10^6$, the boundary layer is laminar. The drop in discharge coefficient, attributed to transition, is progressive over the range $Re_t = [1 \cdot 10^6 - 2 \cdot 10^6]$. It then increases again in the turbulent regime $Re_t > 2 \cdot 10^6$. The N factor associated to this nozzle is continuoulsy increasing from $N = 4.3$ at $Re_t = 10^5$ to $N = 9$ at $Re_t = 10^7$. In this comparison, the transition has occurred at $N \approx 7$.

The N factor calculation is repeated for other R/D and presented in Figure 8. At a given Reynolds number, the N factor increases with R/D as a result of a thicker boundary layer at the nozzle throat.

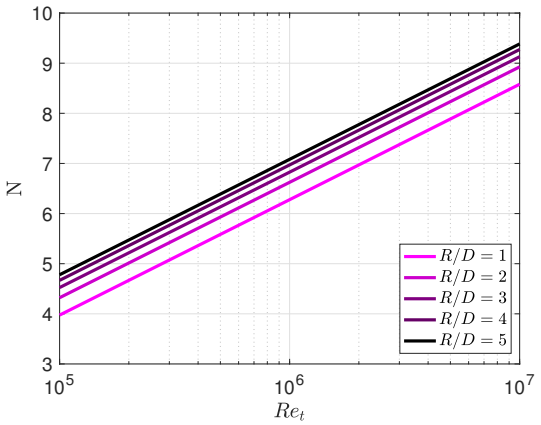

Figure 8. N factor as a fonction of Re_t for various nozzle ratio R/D

In a scenario where the transition occurs at a fixed N factor, the lower R/D, the higher the transition Reynolds number will be. The higher acceleration associated with smaller R/D tends to stabilise the non-modal mechanism. This trend is in accordance with the experiments of Ishibashi (2015), where the higher R/D showed an earlier transition.

THE DISTURBANCES ORIGINS

The spatial transient-growth analysis is based on the optimal disturbance theory, where we have selected the optimal perturbation in order to maximize energy growth. An insight into the possible origins of disturbances is necessary to complete the analysis. There are two main candidates: the first is freestream forcing due to the turbulence that naturally occurs in any flow. The second is wall roughness, where distributed or isolated roughness elements can introduce disturbances in their wake.

Freestream disturbances

Among the experiments conducted by Ishibashi (2015), the discharge coefficients of two nozzles of the same geometry were compared using two different configurations. In the first, the standard shape of Figure 1 was used. In the second, an obstacle is introduced upstream of the nozzle, as shown in Figure 9

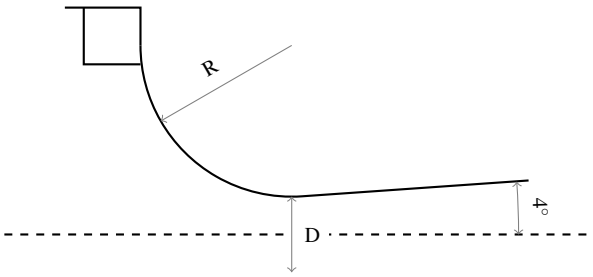

Figure 9. Nozzle with obstacle

The nozzles were mirror polished to eliminate roughness effects on transition. The transition Reynolds number was lower when the obstacle was introduced. Although no quantitative measurements were carried out, the earlier transition was suggested to be related to upstream conditions, such as geometry and disturbances. We can further add that the modifications made on the tested nozzles do not modify the laminar boundary layer profile, as the discharge coefficient in the laminar regime remained unaffected by the changes in geometry. The present analysis suggests that the modified geometry introduces disturbances into the boundary layer. Since the base flow is believed to be the same for both nozzles, the transition mechanism we discuss in this paper is consistent with the hypothesis of Ishibashi. This also suggests that the turbulence intensity of the incoming flow may influence the transition Reynolds number, despite the strongly favorable pressure gradient in the converging section of the nozzle. This is of importance because this is currently not considered when performing mass flow rate measurement on different facilities that may have different incoming turbulence levels.

Disturbance from isolated roughness

Wall roughness is known to cause transition to turbulence provided it is sufficiently large compared to the thickness of the boundary layer. In a numerical investigation, Bernardini *et al.* (2014) performed a parametric study of boundary layer transition induced by an isolated roughness element. They varied the shape, the height, the Reynolds number, and the Mach number and found that a Reynolds number Re_{2k} based on the height of the roughness elements k, the velocity u_k and density

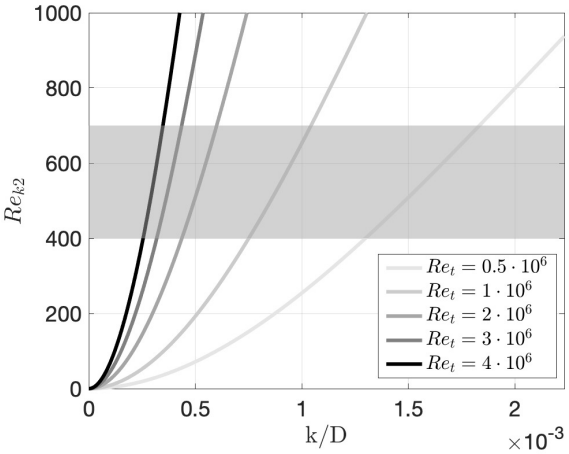

Figure 10. Evolution of the roughness based Reynolds number Re_{2k} as a function of roughness height k/D. The shaded area represents the expected critical Re_{2k} above which the wake behind the roughness element becomes turbulent. Different curves are for different flow conditions Re_t.

ρ_k evaluated in the undisturbed boundary layer at the height k and the viscosity evaluated at wall μ_k

$$Re_{2k} = \frac{\rho_k u_k k}{\mu_k} \tag{16}$$

is convenient to describe the critical roughness height that will cause transition to turbulence. Depending on the roughness shape, the wake introduced behind the obstacle would breakdown to turbulence if $Re_{2k} > [400 - 700]$. Using the analytical formulation of the boundary layer profile we consider, it is possible to calculate this Reynolds number as a function of the roughness height, and thus to determine the critical roughness height as a function of Re_t.

Figure 10 presents Re_{2k} at the nozzle throat as a function of roughness height for five Re_t. We note that at constant Re_{2k}, as Re_t is increased, the critical roughness height decreases as a result of a thinner boundary layer. In the range where Ishibashi (2015) observed transition, that is $Re_t = [1 \cdot 10^6 - 2 \cdot 10^6]$, the computed critical roughness height lies somewhere in the range $k/D \simeq [0.5 - 1] \cdot 10^{-3}$, which correspond to $k \simeq [1 - 2] \cdot 10^{-5} m$ when scaled by the nozzle diameter used in the experiments. These values of roughness height are incompatible with the polished surface used. They correspond to the surface quality obtained via sanding with rough sandpaper. When standard polishing techniques are applied, the expected height of the peaks of roughness is of the order of $k \simeq 1 \cdot 10^{-7}$ m, two orders of magnitude below the minimal transition height estimated. Hence, in that case, it is thought that roughness-induced transition is not the dominant mechanism.

Standard nozzles for mass flow rate measurement are required to have a maximum surface roughness proportional to the throat diameter to reduce effects on the discharge coefficient. This requirement is set at $Ra < 15 \cdot 10^{-6} \times D$, where Ra is the arithmetical mean deviation of the roughness profile z

$$Ra = \frac{1}{l} \int_0^l |z| dx \tag{17}$$

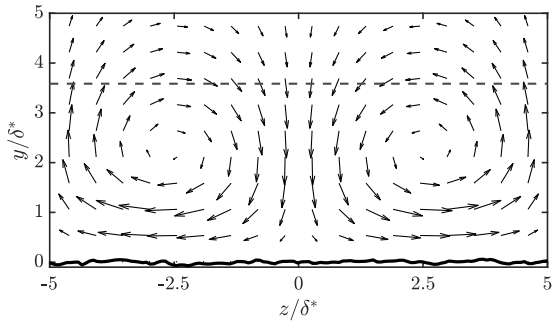

Figure 11. Flow field of the optimal initial disturbance. The dashed line is the boundary layer thickness δ, the black line is the measured wall roughness. $Re_t = 1.75 \cdot 10^6$.

over the length l considered. To ensure that the current analysis is also valid in standard cases and not only applies to mirror-polished nozzles, we perform a roughness study. A piece of aluminum is sanded to meet the roughness required by the norm. The surface roughness is characterized using a Talysurf 6000 CCI (Coherence correlation interferometry) with a wall-normal resolution of $0.01nm$.

The roughness obtained is $Ra = 15 \cdot 10^{-6} \times D$, effectively meeting the requirement. A roughness profile is extracted and compared to an optimal disturbance in Figure 11. It shows that the roughness height is orders of magnitude smaller than the boundary layer thickness and the optimal disturbance. The periodicity of the optimal disturbance is also much larger than that of the roughness profile. The scale separation further indicates that roughness is not the underpinning factor for transition in these configurations.

CONCLUSION

We have used an analytical boundary layer formulation to investigate the transition observed within the throat section of a converging-diverging nozzle. In the locally parallel framework, the stability analysis reveals that transition is not related to a modal mechanism. The T.S. mode is stabilised by the favorable pressure gradient, and no unstable mode is found for nozzle baseflow. Transient-growth analysis shows that significant energy amplification is likely to occur via the lift-up mechanism, which would result in streamwise streaks of low and high speed.

The spatial transient-growth analysis is performed in a parabolized formulation in which upstream-traveling modes are removed. While the gain is proportional to $Re^2_{\delta^*}$, the spatial length at which the maximum gain is achieved is found to scale with the throat diameter. This finding is an important result as it indicates that transient-growth is compatible with the geometry, the spatial length for maximum energy growth being of the order of the nozzle diameter. The optimal gain formulation was used to compute N factors for various nozzle geometries. Comparison with experimental data suggests that non-modal transition occurs at values of $N = 7$, which is lower than the value typically associated with a modal transition. The analysis shows that a smaller inlet in the convergent section will result in delayed transition, indicating that stronger acceleration attenuates non-modal growth mechanisms.

Experimental investigations in the literature have shown that the transition Reynolds number is sensitive to the disturbances injected upstream of the nozzle throat. The current study suggests that the incoming disturbances are amplified via the lift-up mechanism. We have provided an analysis of the potential of isolated roughness-induced transition and shown that it is unlikely to occur for nozzles with surface finish required in industrial configurations. Moreover, the analysis of a sanded surface shows that the surface roughness height distribution is out of scale compared to optimal disturbances. This confirms and strengthens the hypothesis that roughness is not the underpinning factor for transition in these configurations.

REFERENCES

Bernardini, Matteo, Pirozzoli, Sergio, Orlandi, Paolo & Lele, Sanjiva K. 2014 Parameterization of Boundary-Layer Transition Induced by Isolated Roughness Elements **52** (10), 2261–2269.

Bers, A. 1983 Space-time evolution of plasma instabilities-absolute and convective. In *Basic plasma physics.*, , vol. 1. Amsterdam : North-Holland.

Briggs, R.J. 1964 Electron-stream interaction with plasmas. *Tech. Rep.*. MIT Press.

Chu, Boa-Teh 1965 On the energy transfer to small disturbances in fluid flow (Part I) **1** (3), 215–234.

Geropp, D. 1971 Laminare grenzschichten in ebenen und rotationssymmetrischen lavaldsen. In *Deutsche Luft- und Raumfahrt; 71,90*.

Hanifi, A, Schmid, P.J. & Henningson, D.S. 1996 Transient growth in compressible boundary layer flow. *Physics of Fluids* **8** (3), 826–837.

Ishibashi, M. 2015 Discharge coefficient equation for critical-flow toroidal-throat venturi nozzles covering the boundary-layer transition regime. *Flow Measurement and Instrumentation* **44**, 107–121.

Jordan, Peter, Zhang, Mengqi, Lehnasch, Guillaume & Cavalieri, Andr V. 2017 Modal and non-modal linear wavepacket dynamics in turbulent jets. In *23rd AIAA/CEAS Aeroacoustics Conference*. American Institute of Aeronautics and Astronautics.

Mack, L. M. 1984 Boundary layer stability theory. In *AGARD Report No. 709: Special Course on Stability and Transition of Laminar Flow*. AGARD.

Masad, J. A. & Zurigat, Y. H. 1994 Effect of pressure gradient on first mode of instability in compressible boundary layers. *Physics of Fluids* **6** (12), 3945–3953.

Özgen, S. & Kircali, S. A. 2008 Linear stability analysis in compressible, flat-plate boundary-layers. *Theoretical and Computational Fluid Dynamics* **22** (1), 1–20.

Stratford, B. S. 1964 The calculation of the discharge coefficient of profiled choked nozzles and the optimum profile for absolute air flow measurement. *The Journal of the Royal Aeronautical Society* **68** (640), 237245.

Tumin, A. & Reshotko, E. 2001 Spatial theory of optimal disturbances in boundary layers **13** (7), 2097–2104.